Research Square

Preprints are preliminary reports that have not undergone peer review.
They should not be considered conclusive, used to inform clinical practice,
or referenced by the media as validated information.

Tear Proteomics Reveals Metabolic Stress–Driven Ocular Surface Barrier Dysfunction in Myopia

Bin Wu
People's Hospital of Xuancheng City, The Affiliated Xuancheng Hospital of Wannan Medical College
Shenghua Dong
People's Hospital of Xuancheng City, The Affiliated Xuancheng Hospital of Wannan Medical College
Xiaochun Jiang
People's Hospital of Xuancheng City, The Affiliated Xuancheng Hospital of Wannan Medical College
Jiaowen Xu
People's Hospital of Xuancheng City, The Affiliated Xuancheng Hospital of Wannan Medical College
Liufeng Wei
People's Hospital of Xuancheng City, The Affiliated Xuancheng Hospital of Wannan Medical College
Lu Li
159563850870163.com

People's Hospital of Xuancheng City, The Affiliated Xuancheng Hospital of Wannan Medical College
Man She
Eye & ENT Hospital, Fudan University

Article

Keywords: Myopia, Tear proteomics, Ocular surface dysfunction, One-carbon metabolism, Metabolic stress, Corneal epithelial barrier

Posted Date: November 18th, 2026

DOI: https://doi.org/10.21203/rs.3.rs-11316072/v1

License: This work is licensed under a Creative Commons Attribution 4.0 International License.
Read Full License

Additional Declarations: No competing interests reported.

Tear Proteomics Reveals Metabolic Stress–Driven Ocular Surface Barrier Dysfunction in Myopia

Bin Wu[1]， Shenghua Dong[1],Xiaochun Jiang[1],Jiaowen Xu[1],Liufeng Wei[1],Lu Li [2]*,Man She[3*]
1. Department of Ophthalmology, People's Hospital of Xuancheng City, The Affiliated Xuancheng Hospital of Wannan Medical College, Anhui, China.

2.Department of rehabilitation medicine, People's Hospital of Xuancheng City, The Affiliated Xuancheng Hospital of Wannan Medical College, Anhui, China.

3. Department of Ophthalmology, Eye & ENT Hospital, Fudan University,Shanghai 200031, China

* Corresponding authors:
Lu Li. Email: 15956385087@163.com
Man She. Email: sheman11@163.com

Abstract

Background: The global prevalence of myopia is rapidly increasing and has become a major public health concern. Beyond axial elongation and refractive error, accumulating evidence suggests that myopia is associated with ocular surface dysfunction, including tear film instability, epithelial barrier impairment, and altered antimicrobial defense. However, the molecular basis underlying myopia-associated ocular surface imbalance, particularly in pediatric mild-to-moderate myopia, remains incompletely understood.

Methods: In this prospective case–control study, tear samples were collected from 20 children with mild-to-moderate myopia and 20 age- and sex-matched emmetropic controls. Label-free quantitative proteomic profiling was performed using liquid chromatography–tandem mass spectrometry (LC–MS/MS). Differential protein expression analysis, unsupervised clustering, and uniform manifold approximation and projection (UMAP) were conducted following quality control. Functional annotation included Gene Ontology (GO) and Kyoto Encyclopedia of Genes and Genomes (KEGG) pathway enrichment, functional module scoring, correlation network analysis, and protein–protein interaction (PPI) network construction.

Receiver operating characteristic (ROC) analysis was used to evaluate the discriminative performance of key metabolic signatures.

Results: Global tear proteomic profiling revealed a clear separation between mild-to-moderate myopia and control samples, indicating substantial molecular remodeling of the tear film. Myopia exhibited a bidirectional regulatory pattern characterized by upregulation of proteins involved in one-carbon metabolism, nucleotide biosynthesis, and redox homeostasis, together with downregulation of proteins related to corneal epithelial structural maintenance, lysosomal processing, antimicrobial immunity, and vesicular transport. Core enzymes of the one-carbon metabolic pathway, including SHMT1, MTHFD1, and MTHFS, were significantly elevated, accompanied by increased markers of endoplasmic reticulum stress, antioxidant responses, and activation of the STAT1/NF-κB signaling axis. A composite one-carbon metabolism score effectively distinguished myopia from controls (AUC = 0.772). Network analyses further demonstrated coordinated associations among one-carbon metabolism, oxidative stress regulation, interferon signaling, and epithelial structural proteins.

Conclusions: This study delineates a comprehensive tear proteomic landscape in pediatric mild-to-moderate myopia and identifies a metabolic stress–associated ocular surface imbalance characterized by activation of one-carbon metabolism, enhancement of inflammatory signaling, and remodeling of epithelial barrier structure. These findings provide mechanistic insights into ocular surface dysfunction in myopia and suggest potential metabolic biomarkers and therapeutic targets.

Keywords: Myopia; Tear proteomics; Ocular surface dysfunction; One-carbon metabolism; Metabolic stress; Corneal epithelial barrier

1. Background

The global prevalence of myopia has continued to rise and has become a major public health concern worldwide[1,2]. Epidemiological data indicate that myopia is particularly prevalent among children and adolescents in East Asia, and it is projected that approximately half of the global population will be affected by myopia by 2050

[3]. Although myopia exhibits a substantial genetic component, its rapid increase cannot be explained by genetic factors alone. Instead, profound changes in environmental exposure and lifestyle are widely regarded as key driving forces [4]. A growing body of evidence has demonstrated that reduced outdoor activity, increased near-work demand (including reading and electronic screen use), intensified educational pressure, and urbanization are closely associated with both the onset and progression of myopia [5].

Beyond axial elongation and refractive error, myopia is increasingly recognized as a condition accompanied by broader alterations in ocular tissue architecture, metabolic homeostasis, and ocular surface integrity [6]. In recent years, multiple studies have reported that individuals with myopia are more prone to dry eye symptoms, shortened tear break-up time, reduced corneal sensitivity, and increased susceptibility to ocular infection, suggesting that myopia—particularly in its advanced stages—may involve dysregulation of ocular surface immune barriers and tissue homeostasis [7].

As the primary biological interface between the eye and the external environment, ocular surface integrity depends on the coordinated maintenance of corneal epithelial structural proteins, cell–cell adhesion complexes, antimicrobial defense molecules, stromal architecture, and the tear film microenvironment [8]. Tear fluid not only serves essential lubricative and immune-protective functions but also represents a dynamic secretory medium that sensitively reflects cellular stress responses, metabolic states, and tissue injury–repair processes at the ocular surface [9]. Compared with invasive tissue sampling, tear fluid therefore provides an ideal, noninvasive window for biomarker discovery, disease stratification, and mechanistic investigation.

Although previous studies have examined inflammatory mediators, oxidative stress markers, and selected proteins in the tears of patients with myopia, existing evidence has largely focused on individual molecules or isolated pathways. Comprehensive proteomic analyses that delineate the global molecular landscape of the ocular surface microenvironment in low-to-moderate myopia remain limited [10,11]. In particular, whether metabolic reprogramming contributes to myopia-associated ocular surface imbalance, and whether metabolic activation is mechanistically linked to immune

dysfunction and structural barrier deterioration, remain critical but insufficiently explored questions.

Our preliminary proteomic analyses revealed a striking bidirectional dysregulation pattern in the tear proteome of patients with low-to-moderate myopia. On the one hand, proteins involved in one-carbon metabolism, small-molecule metabolism, nucleotide biosynthesis, and protein folding–related stress responses were markedly upregulated, indicating sustained metabolic burden and activation of cellular stress pathways at the ocular surface. On the other hand, proteins associated with corneal epithelial structural maintenance, antimicrobial defense, lysosomal degradation, and glycosphingolipid modification networks were significantly downregulated, reflecting compromised barrier integrity and attenuated innate immune defense. This characteristic molecular profile suggests the presence of a previously unrecognized pathological state in low-to-moderate myopia, which we term “metabolic stress–driven ocular surface remodeling.”

Taken together, the tear proteomic signatures identified in the present study not only provide a novel framework for understanding ocular surface dysfunction in low-to-moderate myopia but also highlight a potential molecular axis linking metabolic stress, barrier impairment, and immune attenuation. These findings may have important implications for future therapeutic strategy development, risk stratification, and disease prediction.

2. Materials and Methods

2.1 Study Design and Participants

This prospective case–control study was designed to characterize tear proteomic alterations associated with pediatric mild-to-moderate myopia. Participants were consecutively recruited from the Department of Ophthalmology, The Second Affiliated Hospital of Anhui Medical University, between January and December 2025.Eligible children were classified into a mild-to-moderate myopia group and an emmetropic control group based on cycloplegic refraction. Forty participants were enrolled (20 per group). Age and sex were recorded at baseline and compared between groups to ensure demographic balance.Despite our frequency-matching strategy,

chronological age differed significantly between groups after consecutive subject enrolment; accordingly, age was regarded as a potential confounding factor in interpreting proteomic findings.The study protocol adhered to the Declaration of Helsinki and was approved by the Ethics Committee of the Affiliated Xuancheng Hospital of Wannan Medical College (approval No.: 2025-1w019-01). The study was conducted under the institutional research project AF-SOP-29-1.0. Written informed consent was obtained from all participants and their legal guardians prior to enrollment.The ophthalmologist performing examinations was an operator rather than a research subject, so separate informed consent for this operator was not required.

2.2 Eligibility Criteria

2.2.1 Inclusion Criteria

Participants were eligible if they fulfilled all of the following criteria:

（1）Age between 5 and 15 years;

(2）Ability to cooperate with ophthalmic examinations and tear sampling procedures;

（3）Clear ocular media and no evidence of active ocular surface disease or infection;

（4）For the myopia group: cycloplegic spherical equivalent (SE) between −6.00 D and −0.50 D in at least one eye;

(5）For the control group: cycloplegic spherical equivalent between −0.50 D and +0.50 D in both eyes.

2.2.2 Exclusion Criteria

（1）Participants were excluded if any of the following were present:

(2）History of ocular disease (including keratitis, uveitis, glaucoma, cataract, or retinal pathology);

（3）Previous ocular surgery or trauma;

（4）Contact lens or orthokeratology lens use within the preceding 3 months;

（5）Systemic inflammatory, autoimmune, or metabolic diseases;

（6）Use of topical or systemic medications known to affect tear composition or ocular surface homeostasis within the preceding month;

（7）Acute ocular infection, allergic conjunctivitis, or pronounced reflex tearing on the day of sampling.

2.3 Ophthalmic Examination Protocol

All ophthalmic examinations were conducted by a single experienced ophthalmologist under standardized conditions to minimize inter-observer variability.Uncorrected visual acuity was measured using a logMAR chart. Cycloplegia was induced following the departmental pediatric protocol, and refractive status was measured after adequate cycloplegia. Spherical equivalent was calculated as SE = sphere + 0.5 × cylinder.Ocular biometric parameters were obtained using the IOLMaster (Carl Zeiss Meditec, Germany). For each parameter, three consecutive measurements were obtained, and the mean value was used for analysis.

2.4 Tear Collection and Pre-Analytical Handling

Tear samples were collected between 9:00 and 11:00 a.m. to minimize circadian variation. Participants were instructed to avoid eye rubbing and topical medication use for at least 2 hours prior to sampling.Tears were collected using sterile Schirmer I filter strips without topical anesthesia. The strip was placed at the lateral third of the lower conjunctival sac for 5 minutes. The wetted portion was excised and transferred into pre-labeled microcentrifuge tubes.Samples were placed on ice immediately after collection and transferred to −80 °C within 30 minutes. Tear proteins were eluted from the strips in cold buffer, followed by centrifugation to remove debris. Samples were processed in randomized batches to minimize batch effects.

2.5 Proteomic Workflow

Protein concentration was quantified using the bicinchoninic acid assay. Equal amounts of protein from each sample were reduced, alkylated, and digested with sequencing-grade trypsin overnight.Peptides were desalted using C18 solid-phase extraction cartridges and analyzed by nanoLC–MS/MS on a high-resolution Orbitrap mass spectrometer operating in data-dependent acquisition mode. Instrument performance was monitored using pooled quality control samples injected at regular intervals.

2.6 Data Processing and Bioinformatics Analysis

Raw MS files were processed using MaxQuant software and searched against the UniProt human protein database. A false discovery rate of 1% was applied at the

peptide and protein levels.Label-free quantification intensities were log2-transformed and normalized. Missing values were imputed from a low-intensity distribution. Differential protein abundance was assessed using moderated linear models with Benjamini–Hochberg correction. Proteins with |log2 fold change| > 1 and adjusted $P < 0.05$ were considered significant.Functional enrichment analyses were performed using Gene Ontology, KEGG[12,13], and Reactome databases. Protein–protein interaction networks were constructed using STRING and visualized in Cytoscape.

2.7 Quality Control and Bias Reduction

Quality control metrics included peptide identification rates, mass accuracy, retention time stability, and coefficient of variation across samples. Principal component analysis and hierarchical clustering were used to detect outliers.Sample processing and data analysis were performed blinded to group allocation.

2.8 Statistical Analysis

Statistical analyses were performed using R software. Continuous variables are presented as mean ± SD or median (interquartile range). Between-group comparisons were performed using independent-samples t tests or Mann–Whitney U tests as appropriate. Categorical variables were compared using chi-square or Fisher's exact tests. A two-sided P value < 0.05 was considered statistically significant.

3.Result

3.1 Baseline ophthalmic characteristics

The baseline ophthalmic characteristics of the low-to-moderate myopia and control groups are summarized in Table 1.Baseline demographic, refractive, and biometric characteristics of the study participants

A total of 40 participants were included in the study, with 20 subjects in the non-myopia group and 20 in the myopia group (Table 1). The myopia group was significantly older than the non-myopia group (9.10 ± 1.80 vs. 6.85 ± 1.79 years, $P = 0.0003$), and also showed greater height and weight (both $P < 0.01$). There were no significant differences in sex distribution between the two groups ($P = 0.747$).

Regarding ocular biometric parameters, axial length and anterior chamber depth were significantly greater in the myopia group (both $P < 0.01$), whereas lens thickness was

slightly reduced (P = 0.023). No significant differences were observed in central corneal thickness, keratometry values (K1 and K2), astigmatism, white-to-white distance, or pupil diameter (all P > 0.05).As expected, the myopia group exhibited significantly lower uncorrected visual acuity and more negative spherical and spherical equivalent refractive errors compared with the non-myopia group (all P < 0.001), while cylinder power did not differ significantly between groups (P = 0.416).

Table 1. Baseline demographic, refractive and ophthalmic characteristics of the study participants

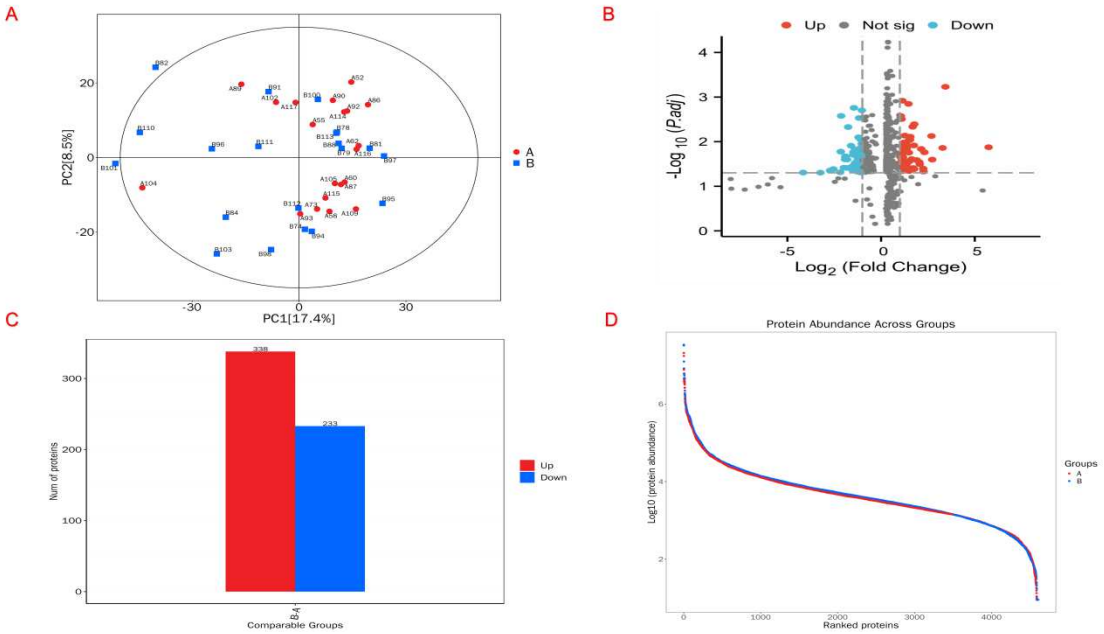
Variable	Non-myopia group (n = 20)	Myopia group (n = 20)	Statistic	P value
Demographic characteristics				
Age (years)	6.85 ± 1.79	9.10 ± 1.80	t = 3.97	0.0003
Male, n (%)	13 (65.0)	11 (55.0)	$\chi^2 = 0.10$	0.747
Female, n (%)	7 (35.0)	9 (45.0)	—	—
Height (m)	1.27 ± 0.12	1.42 ± 0.14	t = 3.47	0.0013
Weight (kg)	26.40 ± 6.14	37.25 ± 9.88	t = 4.17	0.0002
Ophthalmic biometric parameters				
Axial length (AL, mm)	22.84 ± 0.96	24.22 ± 0.88	t = 4.72	<0.001
Central corneal thickness (CCT, μm)	547.75 ± 47.52	533.75 ± 21.90	t = −1.20	0.242

Anterior chamber depth (AD, mm)	2.95 ± 0.23	3.17 ± 0.22	t = 3.08	0.004
Lens thickness (LT, mm)	3.57 ± 0.17	3.43 ± 0.21	t = −2.37	0.023
Keratometry K1 (D)	42.79 ± 1.38	42.39 ± 1.53	t = −0.86	0.394
Keratometry K2 (D)	44.06 ± 1.76	43.54 ± 1.61	t = −0.97	0.339
Astigmatism (AST, D)	1.31 ± 0.80	1.14 ± 0.42	t = −0.84	0.408
White-to-white distance (WTW, mm)	11.91 ± 0.72	12.10 ± 0.40	t = 1.04	0.307
Pupil diameter (PD, mm)	4.82 ± 0.91	4.75 ± 0.54	t = −0.31	0.757
Refractive parameters				
Uncorrected visual acuity (UCVA)	0.81 ± 0.20	0.36 ± 0.20	t = −7.14	<0.001
Sphere (D)	1.21 ± 0.81	−1.23 ± 0.62	t = −10.65	<0.001
Cylinder (D)	−0.56 ± 0.61	−0.44 ± 0.29	t = 0.83	0.416
Spherical equivalent (SE, D)	0.93 ± 0.64	−1.44 ± 0.61	t = −12.06	<0.001

3.2 Proteomic alterations between the myopia and control groups

As shown in Figure 1A, principal component analysis (PCA) based on the quantified proteome revealed a clear separation between the myopia and control groups along the first two principal components, which explained 17.4% and 8.5% of the total variance, respectively, indicating distinct global proteomic profiles between the two

groups. Differential expression analysis identified 571 significantly altered proteins between the two groups, including 338 upregulated and 233 downregulated proteins in the myopia group (Fig. 1B and 1C). The volcano plot (Fig. 1B) showed that the differentially expressed proteins were distributed across a wide range of fold changes, with both upregulated and downregulated proteins observed relative to controls. The bar plot (Fig. 1C) summarizes the number of upregulated and downregulated proteins. The ranked abundance distribution curves (Fig. 1D) demonstrated highly similar overall protein abundance profiles between the two groups, indicating that the observed differences were not driven by global shifts in protein expression. Visualization of the top differentially expressed proteins using a radar plot (Fig. 1E) highlighted several proteins with pronounced changes, with Q8N1Q1 exhibiting the largest fold change among the top candidates. Hierarchical clustering based on differentially expressed proteins (Fig. 1F) showed that samples clustered primarily according to group assignment rather than individual variability, confirming the consistency and robustness of the proteomic differences between the myopia and control groups.



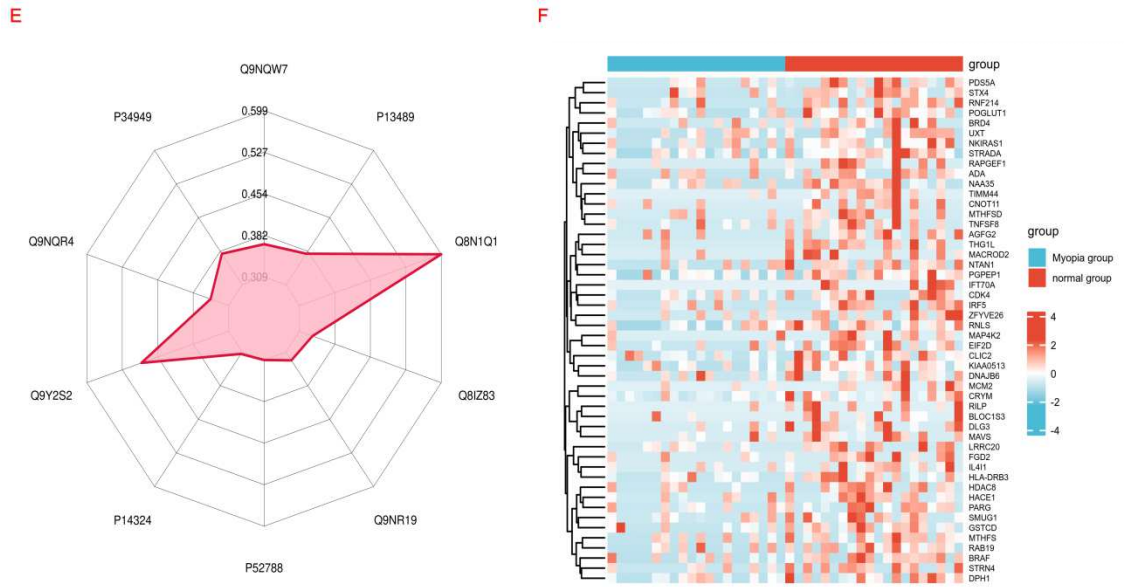
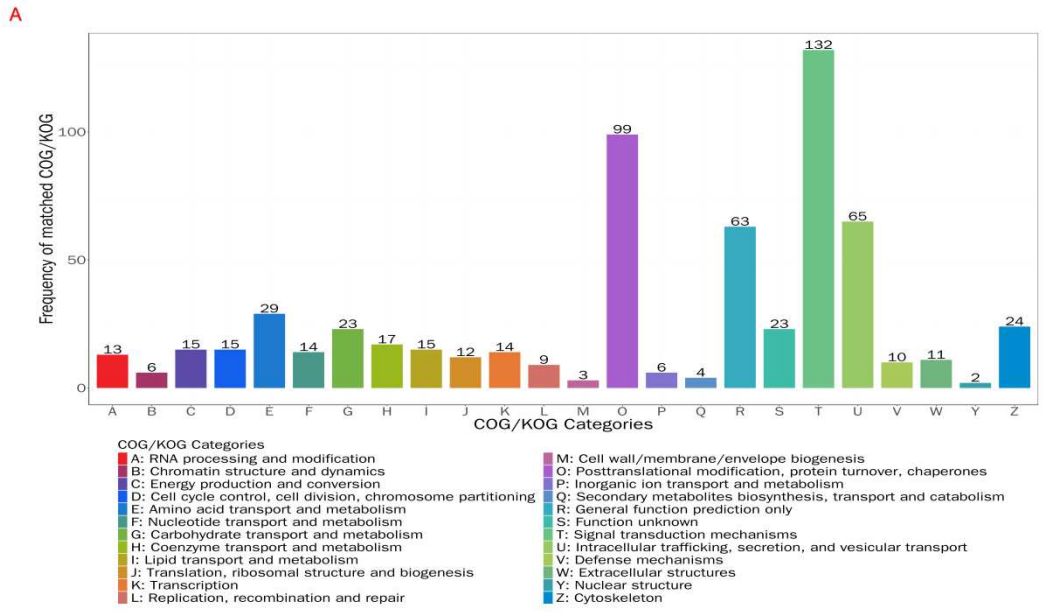


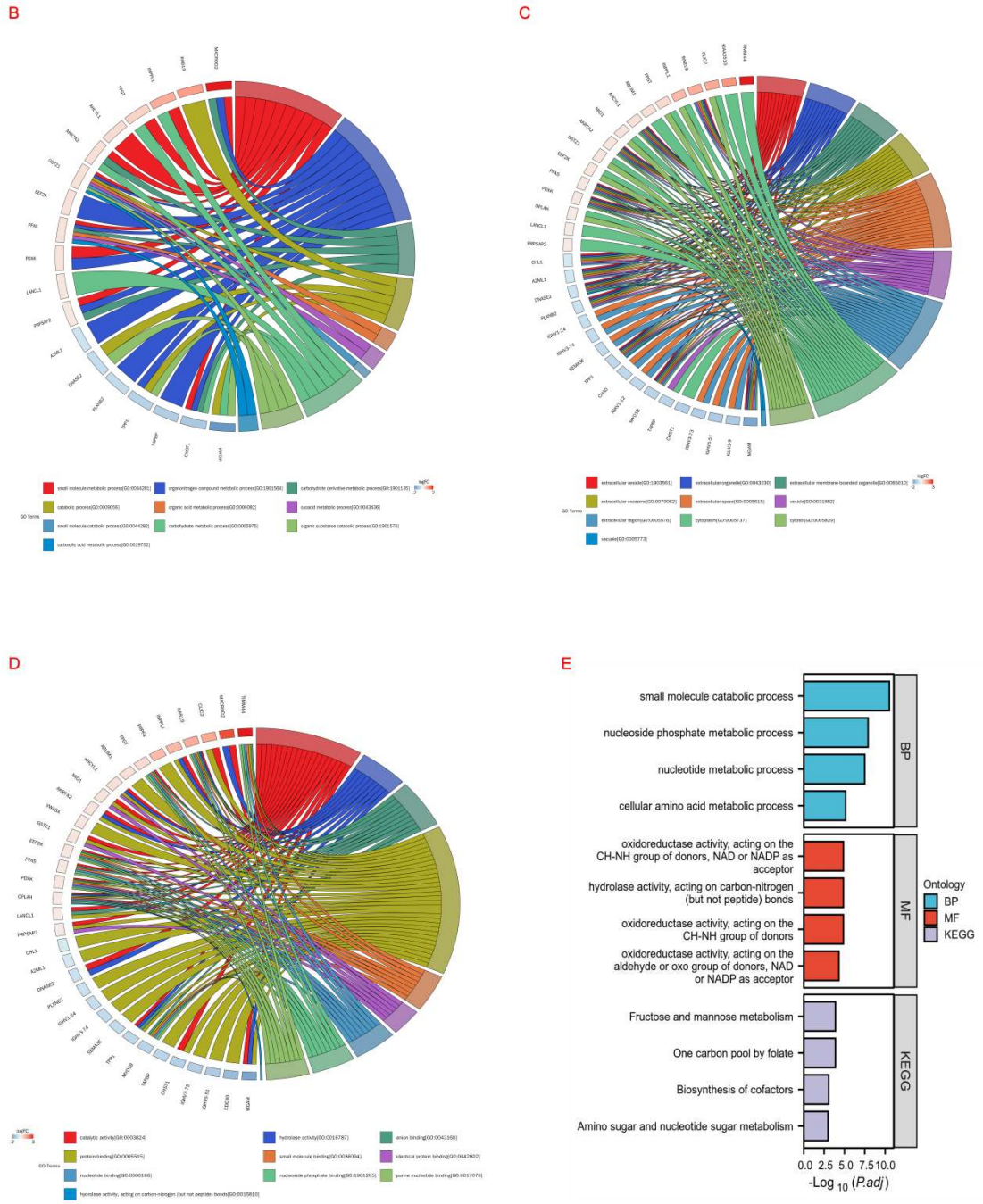
Figure 1. Proteomic profiling of the myopia and control groups.(A) Principal component analysis (PCA) of quantified proteins showing separation between the myopia group (red) and the control group (blue).(B) Volcano plot of differentially expressed proteins between the two groups. Red dots indicate upregulated proteins, blue dots indicate downregulated proteins, and gray dots indicate non-significant proteins.(C) Bar plot showing the number of upregulated and downregulated proteins.(D) Ranked abundance distribution of quantified proteins in the two groups.(E) Radar plot showing the top differentially expressed proteins based on fold change.(F) Heatmap and hierarchical clustering of differentially expressed proteins across samples.

3.3 Functional enrichment and domain characterization of differentially expressed proteins

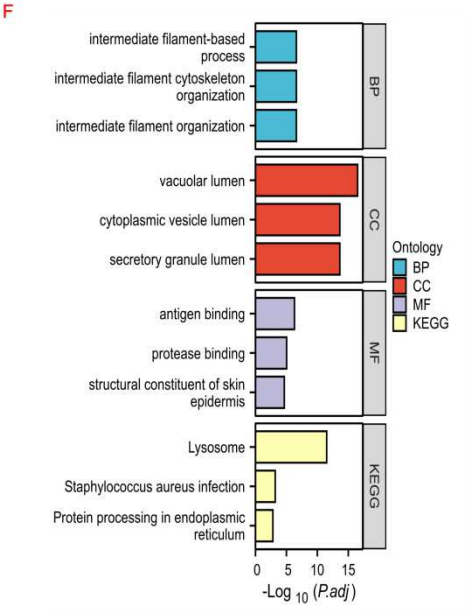
Functional enrichment analysis was performed to characterize the biological functions of differentially expressed proteins (Fig. 2). COG/KOG classification indicated that these proteins were mainly enriched in signal transduction mechanisms (T), posttranslational modification and protein turnover (O), intracellular trafficking and vesicular transport (U), and general function prediction only (R) (Fig. 2A). Gene Ontology analysis showed significant enrichment in small molecule, nucleotide, nucleoside phosphate, and amino acid metabolic processes (BP), as well as

predominant localization to extracellular vesicles, cytoplasm, cytosol, and vesicle-related compartments (CC), and functional association with catalytic activity, hydrolase activity, oxidoreductase activity, and small molecule or nucleotide binding (MF) (Fig. 2B–D). KEGG pathway analysis revealed enrichment in fructose and mannose metabolism, one carbon pool by folate, biosynthesis of cofactors, and amino sugar and nucleotide sugar metabolism pathways (Fig. 2E). Additional enrichment was observed for intermediate filament organization, vacuolar and secretory granule lumen, antigen binding, lysosome, and protein processing in the endoplasmic reticulum (Fig. 2F). Domain and InterPro analyses further demonstrated significant enrichment of immunoglobulin-like folds, WD40 repeat-containing domains, P-loop NTP hydrolase domains, protein kinase-like domains, NAD(P)-binding domains, intermediate filament domains, and aldehyde dehydrogenase-related domains (Fig. 2G and 2H). Together, these results indicate that the dysregulated proteome is primarily associated with metabolic regulation, vesicle-mediated transport, enzymatic activity, cytoskeletal organization, and immune- and secretion-related structural features.

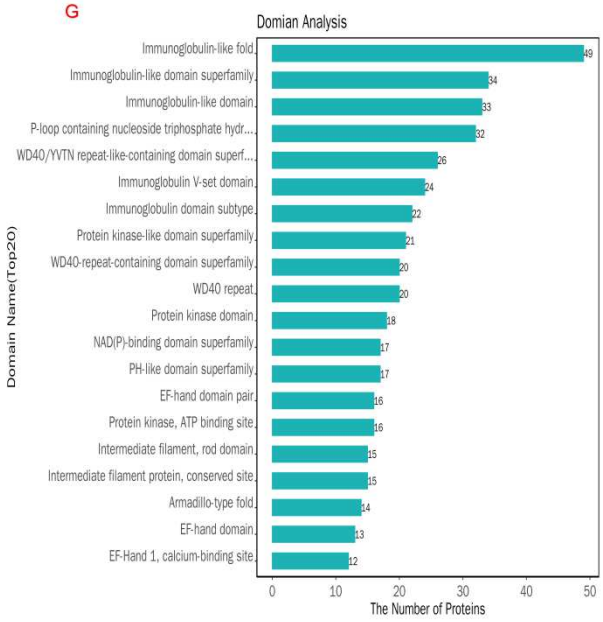



B
C
D
E
small molecule catabolic process
nucleoside phosphate metabolic process
nucleotide metabolic process
cellular amino acid metabolic process
oxidoreductase activity, acting on the CH-NH group of donors, NAD or NADP as acceptor
hydrolase activity, acting on carbon-nitrogen (but not peptide) bonds
oxidoreductase activity, acting on the CH-NH group of donors
oxidoreductase activity, acting on the aldehyde or oxo group of donors, NAD or NADP as acceptor
Fructose and mannose metabolism
One carbon pool by folate
Biosynthesis of cofactors
Amino sugar and nucleotide sugar metabolism
BP
MF
KEGG
Ontology
0.0 2.5 5.0 7.5 10.0
-Log 10 (P.adj)

F


intermediate filament-based process
intermediate filament cytoskeleton organization
intermediate filament organization
vacuolar lumen
cytoplasmic vesicle lumen
secretory granule lumen
antigen binding
protease binding
structural constituent of skin epidermis
Lysosome
Staphylococcus aureus infection
Protein processing in endoplasmic reticulum
BP
CC
MF
KEGG
Ontology
BP
CC
MF
KEGG
0 5 10 15
-Log 10 (P.adj)

G


Domian Analysis
Immunoglobulin-like fold
Immunoglobulin-like domain superfamily
Immunoglobulin-like domain
P-loop containing nucleoside triphosphate hydr...
WD40/YVTN repeat-like-containing domain superf...
Immunoglobulin V-set domain
Immunoglobulin domain subtype
Protein kinase-like domain superfamily
WD40-repeat-containing domain superfamily
WD40 repeat
Protein kinase domain
NAD(P)-binding domain superfamily
PH-like domain superfamily
EF-hand domain pair
Protein kinase, ATP binding site
Intermediate filament, rod domain
Intermediate filament protein, conserved site
Armadillo-type fold
EF-hand domain
EF-Hand 1, calcium-binding site
49
34
33
32
26
24
22
21
20
20
18
17
17
16
16
15
15
14
13
12
Domain Name(Top20)
0 10 20 30 40 50
The Number of Proteins

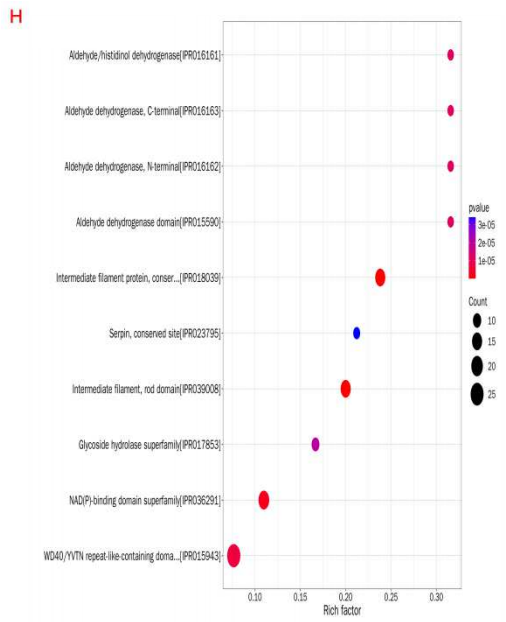


Figure 2. Functional enrichment and domain characterization of differentially expressed proteins.(A) COG/KOG functional classification of differentially expressed proteins.(B) Chord diagram showing enriched Gene Ontology biological process (BP) terms and their associated proteins.(C) Chord diagram showing enriched Gene Ontology cellular component (CC) terms and their associated proteins.(D) Chord diagram showing enriched Gene Ontology molecular function (MF) terms and their associated proteins.(E) Bar plot summarizing the most significantly enriched GO and KEGG terms based on adjusted P values.KEGG pathway enrichment analysis was performed using the clusterProfiler R-package based on the KEGG database resource.(F) Bar plot showing additional enrichment of cytoskeleton-, vesicle-, and immune-related GO and KEGG terms.(G) Bar plot of the most frequent protein domains among differentially expressed proteins.(H) Bubble plot showing significantly enriched InterPro domains, where bubble size indicates the number of proteins and color represents adjusted P value.

3.4 Activation of one-carbon metabolism and stress-response pathways in myopia

To further characterize the molecular features underlying myopia, we examined the expression of representative genes involved in one-carbon metabolism, endoplasmic reticulum (ER) stress, oxidative damage, inflammatory signaling, and cytoskeletal

organization (Fig. 3). Core enzymes of one-carbon metabolism, including SHMT1, MTHFD1, and MTHFS, were significantly upregulated in the myopia group compared with controls (Fig. 3A). ER stress–related genes such as DNAJB6, FKBP9, and SELENBP1 also showed significantly increased expression in the myopia group (Fig. 3B). Genes associated with oxidative damage and redox regulation, including TXNRD1, PRDX6, GPX1, ALDH1L1, and PGD, were markedly elevated in myopic samples (Fig. 3C). Inflammatory signaling components within the STAT1/NF-κB pathway, including STAT1, REL, IKBKE, SYK, IRF5, and NAMPT, were significantly increased in the myopia group (Fig. 3D). In addition, multiple keratin family members (KRT7, KRT8, KRT19, KRT13, and KRT23) exhibited altered expression, indicating cytoskeletal remodeling in myopia (Fig. 3E). Finally, a composite one-carbon metabolism score demonstrated good discriminative performance for distinguishing myopia from control samples, with an area under the ROC curve (AUC) of 0.772 (95% CI, 0.625–0.920) (Fig. 3F).

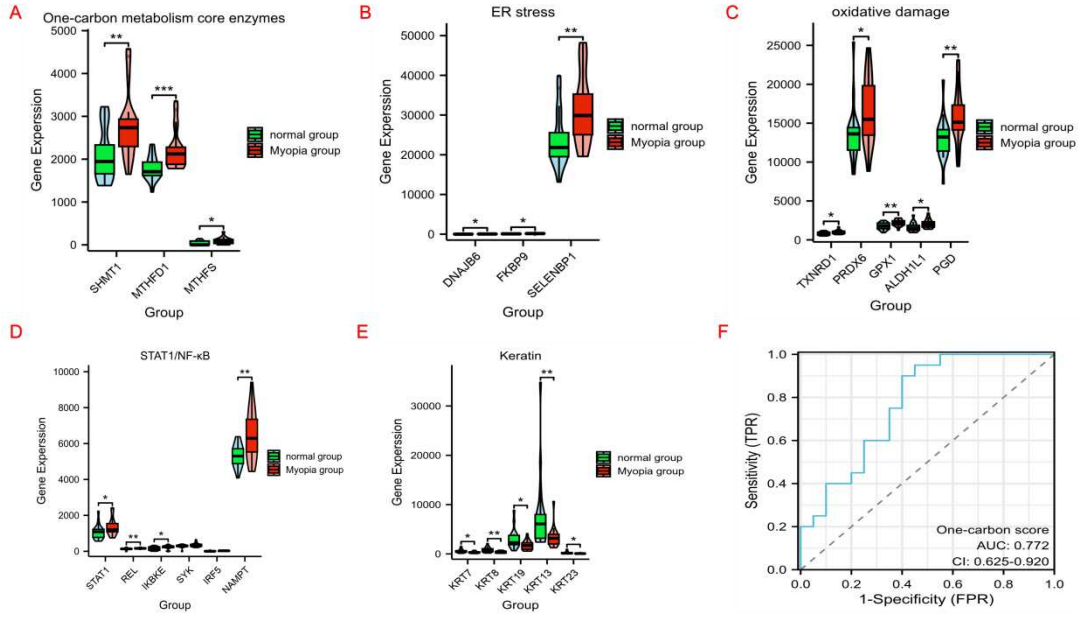


Figure 3. Activation of one-carbon metabolism and stress-response pathways in myopia.(A) Expression of core one-carbon metabolism enzymes (SHMT1, MTHFD1, and MTHFS) in the myopia and control groups.(B) Expression of ER stress–related genes (DNAJB6, FKBP9, and SELENBP1).(C) Expression of oxidative damage and redox-related genes (TXNRD1, PRDX6, GPX1, ALDH1L1, and PGD).(D)

Expression of inflammatory signaling genes in the STAT1/NF-κB pathway (STAT1, REL, IKBKE, SYK, IRF5, and NAMPT).(E) Expression of keratin family genes associated with cytoskeletal organization (KRT7, KRT8, KRT19, KRT13, and KRT23).(F) Receiver operating characteristic (ROC) curve showing the performance of the one-carbon metabolism score for discriminating myopia from controls.

3.5 One-carbon metabolism is coordinately associated with epithelial remodeling and cellular stress responses in myopia

To explore the coordinated regulation between one-carbon metabolism and epithelial and stress-response programs in myopia, we performed correlation and expression stratification analyses focusing on one-carbon metabolic enzymes, keratin family members, ER stress markers, oxidative stress genes, and inflammatory regulators. Circular correlation analysis showed that SHMT1, MTHFD1, and MTHFS were strongly associated with multiple keratins, including KRT5, KRT7, KRT8, KRT10, KRT13, KRT19, and KRT23 (Fig. 4A). These enzymes also exhibited significant correlations with epidermal differentiation–related genes such as SPRR family members and TGM1 (Fig. 4B), as well as cytoskeletal and adhesion-associated genes including PLEC, UTRN, and MYO1B (Fig. 4C). An integrated correlation network further revealed widespread associations among one-carbon metabolism enzymes, ER stress markers (DNAJB6, FKBP9, SELENBP1), oxidative stress genes (TXNRD1, PRDX6, GPX1, ALDH1L1, PGD), and inflammatory signaling components (STAT1, REL, IKBKE, SYK, IRF5, NAMPT) (Fig. 4D). Stratification of samples based on SHMT1, MTHFD1, or MTHFS expression demonstrated that higher expression of one-carbon enzymes was accompanied by increased levels of ER stress, oxidative stress, and inflammatory response genes (Fig. 4E–G). In parallel, keratin gene expression patterns showed coordinated shifts between low- and high-expression groups of SHMT1, MTHFD1, and MTHFS (Fig. 4H–J). Together, these analyses indicate that one-carbon metabolic activity is closely linked to epithelial structural remodeling and cellular stress-response programs in myopia.

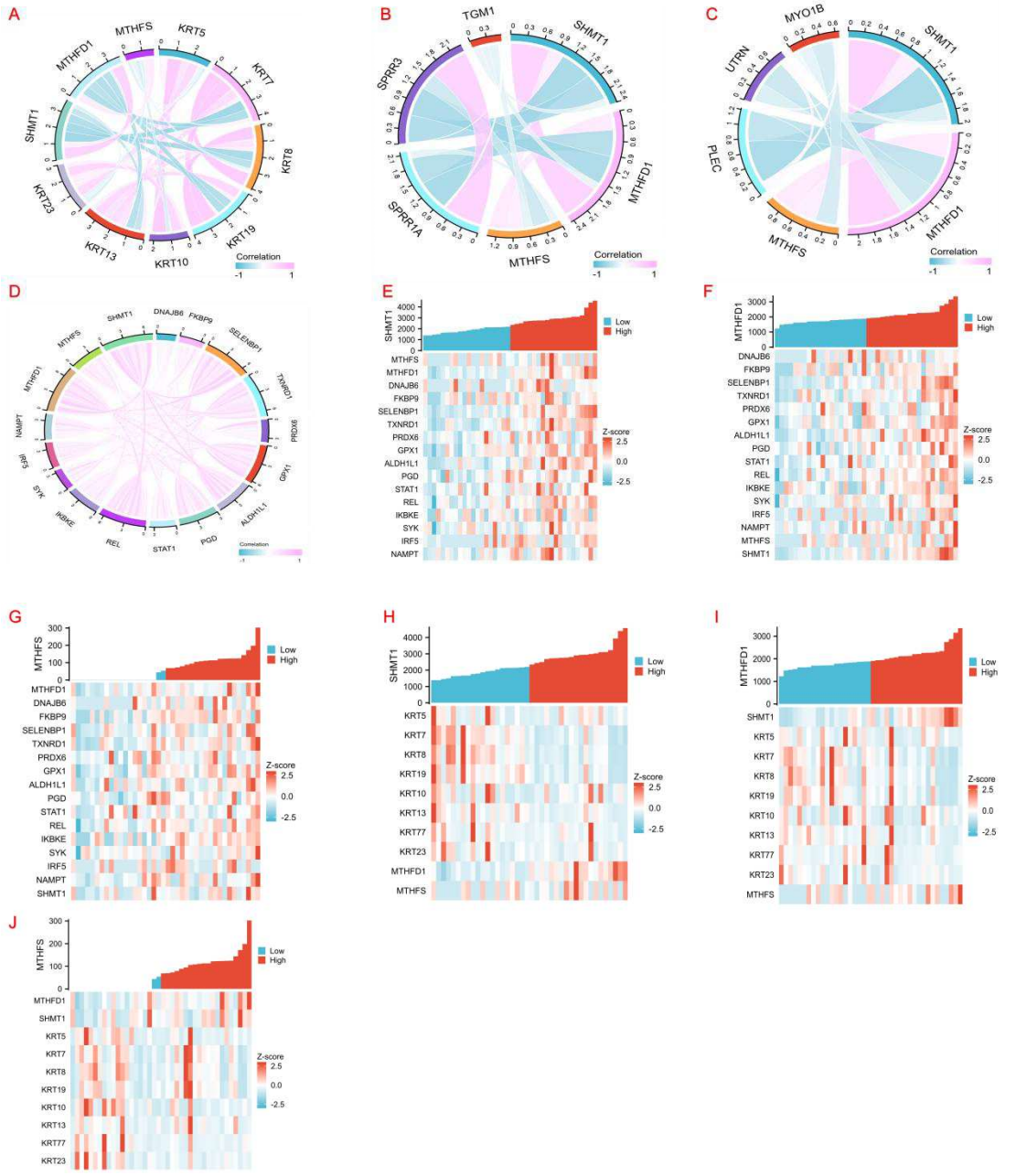


Figure 4. Correlation and stratification analyses reveal coordinated regulation of one-carbon metabolism, epithelial remodeling, and stress-response pathways.(A) Circular correlation between one-carbon metabolism enzymes and keratin family members.(B) Correlations between one-carbon enzymes and epidermal differentiation–related genes (SPRR family and TGM1).(C) Correlations between one-carbon enzymes and cytoskeletal and adhesion-associated genes.(D) Integrated correlation network among one-carbon metabolism, ER stress markers, oxidative stress genes, and inflammatory signaling components.(E–G) Heatmaps of

stress-response and inflammatory gene expression stratified by SHMT1 (E), MTHFD1 (F), and MTHFS (G).(H–J) Heatmaps of keratin gene expression stratified by SHMT1 (H), MTHFD1 (I), and MTHFS (J).

3.6 One-Carbon Metabolism–Centered PPI Network Underlies Cellular Phenotype Remodeling

To characterize the functional organization of the differentially expressed proteins, we constructed a protein–protein interaction (PPI) network(fig.5). The network revealed a highly modular architecture with three major interconnected clusters. The largest cluster was enriched for proteasome and ubiquitin-mediated protein degradation components, including multiple PSMA, PSMB, PSMD, and PSME subunits as well as ADRM1, indicating activation of protein turnover and proteostasis pathways. A central signaling cluster was composed of inflammatory and stress-response regulators such as RELA, NFKB1, STAT1, STAT5B, MAPK1, MAPK3, MAP3K7, MAP3K8, JAK1, NFATC2, KRAS, and RAF1, suggesting coordinated activation of NF-κB, JAK–STAT, and MAPK signaling pathways. In addition, a distinct cluster was enriched for endoplasmic reticulum and glycoprotein processing factors, including SEC61A1, SSR1, MAN1A1, MAN1B1, MOGS, DDOST, CANX, and GANAB, reflecting enhanced protein folding, modification, and secretion processes. Together, these results indicate that the altered proteome is organized into interconnected modules linking proteostasis, stress/inflammatory signaling, and ER-associated protein processing.

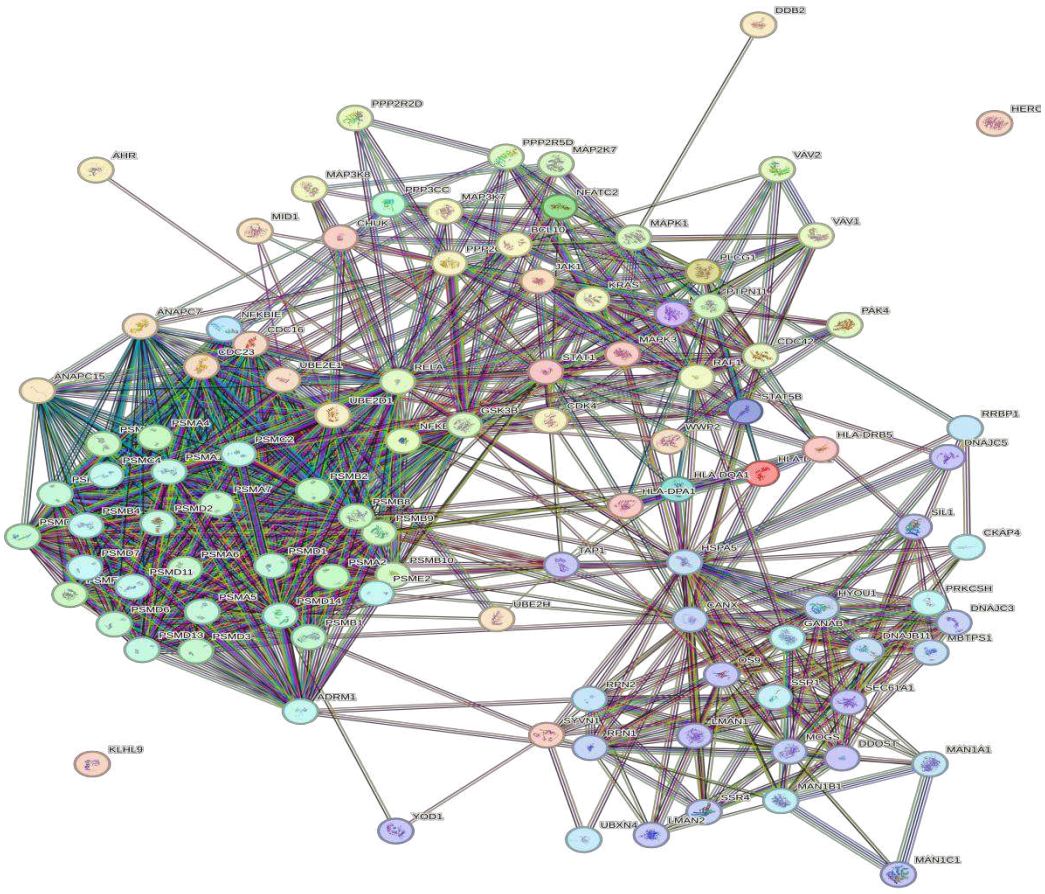


Figure 5. Protein–protein interaction network of differentially expressed proteins. The PPI network was constructed using STRING and visualized in Cytoscape. Three major functional modules were observed, corresponding to proteasome-mediated protein degradation, stress and inflammatory signaling, and endoplasmic reticulum–associated protein processing. Node colors indicate protein identity, and edges represent known or predicted protein–protein interactions.

4. Discussion

In this study, we systematically characterized the expression patterns and network associations of key one-carbon metabolism enzymes in the ocular surface microenvironment associated with low-to-moderate myopia, thereby extending the conventional understanding of this metabolic pathway beyond its classical biochemical roles. Traditionally, one-carbon metabolism has been regarded primarily as a core metabolic module supporting nucleotide biosynthesis, methyl donor cycling,

and redox homeostasis. However, accumulating evidence suggests that this pathway also plays broader regulatory roles in cellular stress adaptation, immune modulation, and tissue remodeling. Our findings further support the concept that one-carbon metabolism may function as a central regulatory hub within a metabolism–structure–immune axis governing tissue homeostasis.

At the network level, SHMT1, MTHFD1, and MTHFS exhibited strong coordinated expression with regulators of oxidative stress, interferon signaling pathways, and epithelial structural components. These observations are consistent with prior studies in cancer biology, chronic inflammatory conditions, and tissue repair, in which enhanced one-carbon metabolism has been shown to increase cellular tolerance to metabolic and oxidative stress by supporting NADPH production, glutathione regeneration, and macromolecule synthesis[14-19]. Extending these concepts beyond tumor contexts, our results suggest that one-carbon metabolism may similarly serve as a metabolic buffer supporting structural stability and stress resilience in non-neoplastic tissues.

From a structural and epithelial homeostasis perspective, elevated expression of one-carbon metabolism genes was accompanied by coordinated upregulation of multiple keratin family members, including KRT5, KRT7, KRT8, KRT13, KRT19, and KRT23. Keratin networks are fundamental determinants of epithelial mechanical integrity and barrier function, and they also serve as sensitive indicators of cellular differentiation status, regenerative capacity, and responses to environmental stress. Previous studies have demonstrated that chronic inflammatory or metabolic stress conditions induce reorganization of keratin networks to reinforce epithelial resilience and barrier defense[20-22]. In line with these findings, we observed significant coupling between one-carbon metabolism genes and differentiation- and cornification-associated molecules such as TGM1 and SPRR family members, supporting the notion that metabolic state transitions may actively participate in initiating epithelial remodeling and barrier reinforcement programs.

Protein–protein interaction analysis further revealed that one-carbon metabolism enzymes occupy highly connected central positions within the network and are

hierarchically linked to protein folding regulators, molecular chaperone systems, and ubiquitin–proteasome degradation pathways. The concept of proteostasis has emerged as a key integrator of metabolic status and cellular functional stability. Under sustained metabolic or oxidative stress, cells increasingly rely on enhanced protein quality control mechanisms to prevent the accumulation of misfolded or damaged proteins that could otherwise compromise cytoskeletal organization and cellular integrity[23,24]. The concurrent upregulation of one-carbon metabolism and proteostasis-related pathways observed in this study suggests the presence of a metabolic adaptation–driven structural protection mechanism that preserves epithelial function under chronic stress conditions.

In addition to its structural associations, one-carbon metabolism was closely linked to immune regulation in the present study. Samples with high expression of one-carbon metabolism genes showed concomitant activation of STAT1-, IRF5-, and IKBKE-mediated signaling, along with coordinated upregulation of antioxidant regulators such as TXNRD1 and PRDX6. These findings align well with previous reports proposing a tight coupling between one-carbon metabolism and immune signaling, in which metabolic flux influences interferon responsiveness, antigen presentation efficiency, and chronic inflammatory sensitivity through regulation of redox balance, NAD^+ availability, and epigenetic modifications[25]. Thus, rather than serving merely as a supplier of biosynthetic substrates, one-carbon metabolism may modulate immune signaling thresholds and inflammatory persistence through its integrated effects on oxidative stress buffering and epithelial barrier status.

Several limitations of this study should be acknowledged. First, although we intended to perform age- and sex-frequency-matching between groups, significant differences in chronological age were still observed between the mild-to-moderate myopia and emmetropic control groups after consecutive enrolment. Age represents a potential confounding variable for tear-protein profiles and ocular-surface physiology in children, which may partly contribute to the observed molecular differences. We could not fully exclude residual age-related effects in the present exploratory cohort. Second, this was a single-centre study with a relatively small sample size (n = 40).

The moderate AUC value of 0.772 for the composite one-carbon-metabolism signature indicates exploratory discriminative capacity rather than mature clinical diagnostic performance; therefore, our biomarker findings require further validation in larger, independent multi-centre paediatric cohorts before any clinical translation. Third, all proteomic and network analyses in this work are correlative. We cannot definitively determine whether elevated one-carbon-metabolic signalling acts as a causal driver of ocular-surface epithelial remodelling and inflammatory activation, or merely represents a compensatory adaptive response triggered by pre-existing epithelial and inflammatory stress. Fourth, key metabolic nodes including SHMT1, MTHFD1 and MTHFS have not been validated through in-vitro cell experiments or in-vivo animal models. Hence, the causal direction of the proposed "metabolic-stress-epithelial-barrier-immune" axis remains unproven. Finally, longitudinal sampling is absent in our cross-sectional case-control design. Whether this molecular regulatory network dynamically changes alongside myopia progression, ocular-surface status or therapeutic intervention deserves further prospective longitudinal investigation.

Collectively, this study expands the biological scope of one-carbon metabolism and highlights its potential role as an integrative hub linking metabolic stress adaptation, epithelial structural remodeling, and immune regulation. The coordinated interaction among one-carbon metabolism, cytoskeletal architecture, and immune signaling provides a novel conceptual framework for understanding tissue homeostasis and pathological remodeling, and may offer new opportunities for metabolic intervention, tissue repair, and precision therapeutic strategies.

5. Conclusions

This study demonstrates that key one-carbon metabolism enzymes extend beyond their canonical roles in nucleotide biosynthesis and methyl donor cycling to participate in epithelial structural stabilization, keratin network remodeling, and immune signal regulation. Through integrative expression profiling and protein interaction network analysis, we show that SHMT1, MTHFD1, and MTHFS are

coordinately linked to cytoskeletal pathways, barrier formation genes, and interferon signaling cascades, positioning one-carbon metabolism as a potential molecular hub connecting metabolic stress adaptation, tissue structural remodeling, and immune modulation. These findings provide new insights into complex tissue homeostasis mechanisms and highlight one-carbon metabolism as a promising target for future metabolic and therapeutic interventions

6. Funding

This study was supported by the the Project of The Affiliated Xuancheng Hospital of Wannan Medical College (Grant No. KY202446). The funding body had no role in the study design, data collection, data analysis, interpretation of the results, or manuscript preparation.

7.Author contributions

B.W. conceived and designed the study, performed ophthalmic examinations, collected clinical samples, and drafted the manuscript. S.D., X.J., J.X. and L.W. participated in subject recruitment, clinical data collection, data analysis and manuscript revision. M.S. and L.L. contributed to study design, supervised the whole research project, and critically revised the manuscript for important intellectual content. All authors read and approved the final version of the manuscript. Competing interests The authors declare no competing interests.

8.Competing interests

The authors declare no competing interests.

9. Data availability statement

The datasets generated and analysed during the current study are not publicly available due to restrictions related to participant privacy and ethical requirements. Reasonable requests for the de-identified minimal dataset can be directed to the corresponding author.

10.References

1.Williams KM, Hammond CJ. Perspectives on genetic and environmental factors in myopia, its prediction, and the future direction of research. Invest Ophthalmol Vis Sci.

2025;66(7):4. doi:10.1167/iovs.66.7.4.

2.Manoharan MK, Tivari UP, Reddy JC, Verkicharla PK. Myopia progression in young adults: insights from real-world clinical data. Clin Exp Optom. 2025;108(7):873–879. doi:10.1080/08164622.2025.2475200.

3.Zhao L, Xie Y, Chen W, Zhang Y, Lu Y, Li Y, Yin Y, Hu T, Wen D. Advancing myopia management: the therapeutic potential of microbiota-targeted interventions. Am J Ophthalmol. 2025;279:34–47. doi:10.1016/j.ajo.2025.07.008.

4.Li DL, Lanca C, Zhang XJ, Grzybowski A, He XG, Pan CW. Spatial frequency of environments and myopia: a systematic review on associated evidence and underlying mechanisms. Acta Ophthalmol. 2025;103(8):909–918. doi:10.1111/aos.17437.

5.Fernández Irigaray L, Torres R, Zanutigh V, Lanca C, Grzybowski A, Iribarren R. Lifestyle and sleep-related behaviours in children with myopia. BMC Ophthalmol. 2025;25(1):97. doi:10.1186/s12886-025-03923-1.

6.Huang Z, Zhou J, Liu S, Zhang Y, Meng J, Zhu X, Du Y. The interplay between systemic inflammation and myopia: A bidirectional Mendelian randomization and experimental validation study. Int Immunopharmacol. 2025;157:114803. doi:10.1016/j.intimp.2025.114803.

7.Xu R, Zheng J, Liu L, Zhang W. Effects of inflammation on myopia: evidence and potential mechanisms. Front Immunol. 2023;14:1260592. doi:10.3389/fimmu.2023.1260592.

8. Xin J, Bao B, Liu J, Ma Z, Zhang M, Bi H, Guo D. Crosstalk between myopia and inflammation: A mini review. Int J Med Sci. 2024;21(9):1589–1603. doi:10.7150/ijms.94826.

9. Nättinen J, Aapola U, Nukareddy P, Uusitalo H. Clinical tear fluid proteomics—A novel tool in glaucoma research. Int J Mol Sci. 2022;23(15):8136. doi:10.3390/ijms23158136.

10.Adigal SS, Rizvi A, Rayaroth NV, John RV, Barik A, Bhandari S, George SD, Lukose J, Kartha VB, Chidangil S. Human tear fluid analysis for clinical applications: progress and prospects. Expert Rev Mol Diagn. 2021;21(8):767–787. doi:10.1080/14737159.2021.1941879.

11.Ponzini E. Tear biomarkers. Adv Clin Chem. 2024;120:69–115. doi:10.1016/bs.acc.2024.03.002.

12.Kanehisa M, Sato Y, Kawashima M, Furumichi M, Tanabe M. KEGG as a reference resource for gene and protein annotation. Nucleic Acids Res. 2016;44(D1):D457-D462. doi:10.1093/nar/gkv1070.

13.Kanehisa M, Goto S. KEGG: kyoto encyclopedia of genes and genomes. Nucleic Acids Res. 2000;28(1):27-30. doi:10.1093/nar/28.1.27

14.Ducker GS, Rabinowitz JD. One-carbon metabolism in health and disease. Cell Metab. 2017;25(1):27-42. doi:10.1016/j.cmet.2016.08.009.

15.Ducker GS, Ghergurovich JM, Mainolfi N, Suri V, Jeong SK, Li SH, et al. Human SHMT inhibitors reveal defective glycine import as a targetable metabolic vulnerability of diffuse large B-cell lymphoma. Proc Natl Acad Sci U S A. 2017;114(43):11404-9. doi:10.1073/pnas.1706617114.

16.Yang L, Garcia Canaveras JC, Chen Z, Wang L, Liang L, Jang C, et al. Serine catabolism feeds NADH when respiration is impaired. Cell Metab. 2020;31(4):809-21.e6. doi:10.1016/j.cmet.2020.02.017.

17.Zheng Y, Liu B, Wang L, Lei H, Pulgar Prieto KD, Pan D. Targeting SHMTs and MTHFDs in cancer: attractive opportunity for anti-tumor strategy. Front Pharmacol. 2024;15:1363786. doi:10.3389/fphar.2024.1363786.

18.Dang L, Su SM. Isocitrate dehydrogenase mutation and (R)-2-hydroxyglutarate: from basic discovery to therapeutics development. Annu Rev Biochem. 2017;86:305-31. doi:10.1146/annurev-biochem-061516-044732.

19.Koseki J, Konno M, Asai A, Colvin H, Kawamoto K, Nishida N, et al. Tumor reliance on cytosolic versus mitochondrial one-carbon flux depends on folate availability. Cell Metab. 2021;33(1):190-8.e3. doi:10.1016/j.cmet.2020.12.002.

20.Pan X, Hobbs RP, Coulombe PA. The expanding significance of keratin intermediate filaments in normal and diseased epithelia. Curr Opin Cell Biol. 2013 Feb;25(1):47-56. doi: 10.1016/j.ceb.2012.10.018.

19.Kumar V, Bouameur JE, Bär J, Rice RH, Hornig-Do HT, Roop DR, et al. A keratin scaffold regulates epidermal barrier formation, mitochondrial lipid composition, and

activity. J Cell Biol. 2015 Nov 23;211(5):1057-75. doi: 10.1083/jcb.201404147.

21. Vetter A, Beier LS, Bouameur JE, Magin TM. Keratins modulate cellular reduction-oxidation homeostasis and mitochondrial dynamics. J Invest Dermatol. 2022 Aug;142(8):2264-2267.e6. doi: 10.1016/j.jid.2022.03.001.

22. Zhang S, Wang M, Wang C, Wang G, Sun K, Xiong S, et al. Intrinsic abnormalities of keratinocytes initiate skin inflammation through the IL-23/T17 axis in a MALT1-dependent manner. J Immunol. 2021 Feb 15;206(4):839-48. doi: 10.4049/jimmunol.2001031.

23. Balchin D, Hayer-Hartl M, Hartl FU. In vivo aspects of protein folding and quality control. Science. 2016 Jul 1;353(6294):aac4354. doi: 10.1126/science.aac4354.

24. Soultanas A, Röwer C, Serrano M. Proteostasis failure in neurodegenerative diseases: focus on oxidative stress. Oxid Med Cell Longev. 2023 Apr 17;2023:1976.

25. Kriegenburg F, Ellgaard L, Hartmann-Petersen R. Molecular chaperones in targeting misfolded proteins for ubiquitin-dependent degradation. FEBS J. 2012 Mar;279(6):532-42. doi: 10.1111/j.1742-4658.2012.08483.x

Supplementary Files

This is a list of supplementary files associated with this preprint. Click to download.

- DIAQuantitativeProteomicsTestReportEnglish.pdf